Title

Turbulence Nonlinearities Shed Light on Geometric Asymmetry in Tokamak Confinement Transitions

Journal

Physical Review Letters, 118(10)

ISSN

0031-9007

Authors

Cziegler, I
Hubbard, AE
Hughes, JW
et al.

Publication Date

2017-03-10

DOI

10.1103/physrevlett.118.105003

Peer reviewed

Turbulence Nonlinearities Shed Light on Geometric Asymmetry in Tokamak Confinement Transitions

I. Cziegler
York Plasma Institute, Department of Physics, University of York, Heslington YO10 5DD, United Kingdom

A. E. Hubbard, J. W. Hughes, and J. L. Terry
Plasma Science and Fusion Center, Massachusetts Institute of Technology, Cambridge, Massachusetts 02139, USA

G. R. Tynan
University of California San Diego, La Jolla, California 92093, USA
(Received 1 November 2016; published 9 March 2017)

A comprehensive study of fully frequency-resolved nonlinear kinetic energy transfer has been performed for the first time in a diverted tokamak, providing new insight into the parametric dependences of edge turbulence transitions. Measurements using gas puff imaging in the turbulent L-mode state illuminate the source of the long known but as yet unexplained "favorable-unfavorable" geometric asymmetry of the power threshold for transition to the turbulence-suppressed H mode. Results from the recently discovered I mode point to a competition between zonal flow (ZF) and geodesic-acoustic modes (GAM) for turbulent energy, while showing new evidence that the I-to-H transition is still dominated by ZFs. The availability of nonlinear drive for the GAM against net heat flux through the edge corresponds very well to empirical scalings found experimentally for accessing the I mode.

DOI: 10.1103/PhysRevLett.118.105003

Turbulent systems are often prone to dynamic changes that can be best described as bifurcations. Examples include the transition to turbulence [1,2], as well as transitions in plasma turbulence [3,4]. In such phase transitions, global structure must be described simultaneously with turbulence. This study is aimed at the analysis of self-organization in turbulent flows and at the dependence of the *type* of transitions on flow-turbulence interactions. In particular, tokamak plasma turbulence is examined in terms of energetic exchanges leading to various transition phenomena.

From a turbulence science perspective, the greatest significance of discovering the high confinement (H mode) regime [3] of tokamak operation was the insight that confinement states exist. As heat and mass transport across the confining magnetic field is dominated by turbulence, confinement regimes correspond to states of turbulence. Since then, a number of "intermediate" regimes have also been discovered, such as the limit-cycle oscillating (LCO) regime [5,6], and the I mode [7,8]. It is known empirically that the H mode develops from low-confinement (L mode) when the heating power exceeds a threshold. To date, no predictive theory has been developed comprehensively to model what parameters determine this threshold. Its widely referenced scaling [9] also neglects some key interrelations which experiments of the past few decades indicated, such as those with plasma rotation [10,11], material of the first wall [12], main species isotope [13], etc.

One of the largest effects among these is that of the up-down asymmetry of single-null diverted magnetic configurations [14]. The power threshold in an equilibrium in which the ion grad-B drift points toward the null of the poloidal field (X point; see Fig. 1 for a typical cross section) is approximately half as high as in the opposite case, i.e., with $\mathbf{B} \times \nabla B$ away from the X point; hence, the former geometry is known as "favorable" and the latter as "unfavorable." Despite its broad reproducibility and importance for turbulence physics as well as reactor operation, the cause of this asymmetry has proven elusive for the past few decades.

This Letter reports on the first comprehensive experimental study directly to address the nonlinear physics in the "favorable-unfavorable" asymmetry in strongly heated

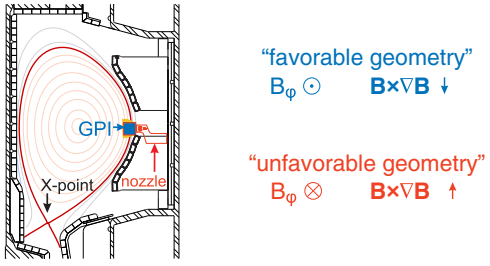

FIG. 1. Cross section of the Alcator C-Mod with a lower-single-null (LSN) equilibrium; the thick (red) line represents the LCFS. Locations of the gas-puff nozzle and GPI views are indicated on the right.

plasmas leading all the way to the transition into the H mode. Frequency-resolved transfer rates of kinetic energy are calculated from gas-puff imaging (GPI) [15,16] measurements. They are compared and distinguished between L-mode plasmas with $\mathbf{B} \times \nabla B$ toward and away from the X point, and contrasted against the I mode. Results point out the importance of flow-turbulence nonlinearities in understanding confinement regimes.

One remarkable feature of the favorable-unfavorable asymmetry is the difference in the intermediate regimes to which each configuration can lead. LCO regimes typically occur in the favorable geometry with heating power just below the threshold. Conversely, the I mode is most easily accessed with an unfavorable grad-B drift, which does not lend itself to LCO. In contrast to LCO, the I mode is a stationary regime, characterized by a separation between heat and mass transport such that it forms a thermal transport barrier while providing little or no barrier to either main ion or impurity particles above the L-mode level. Beyond exciting questions about the underlying statistical physics, this renders the regime highly reactor relevant, since the resulting temperature and confinement can be as high as in the H mode, without impurity accumulation or the excess heat load of edge localized mode (ELM) eruptions. Its edge fluctuations are instead characterized by the "weakly coherent mode" (WCM) and concomitant geodesic acoustic modes (GAM) [17]. Experiments in multiple devices have shown the two to be nonlinearly coupled [18,19] and contemporaneous with the I mode. The window between the L and H mode in which I modes can be accessed is as interesting from a turbulence perspective as it is crucial for exploiting this extremely attractive regime for fusion.

Studies of the LCO yielded instrumental evidence for the role of zonal flows [20] in L-H transitions [6]. Zonal flows (ZF) and GAMs are both linearly stable, axisymmetric, radially sheared $\mathbf{E} \times \mathbf{B}$ flows, driven nonlinearly by turbulence, which thus loses power, and if sufficiently strong this quenching enhances confinement. Hence the limit cycles between the L and H mode have been shown to exhibit predator-prey oscillations. While the ZFs are quasi-zero-frequency modes, GAMs are a finite frequency branch, but otherwise their drive processes may be studied similarly. The specific form of the nonlinearities studied can be understood by considering some topical results about the L-H transition. Figure 2 shows representative histories of some key quantities measured in experiments which recently [21–23] demonstrated the Reynolds-stress-mediated nonlinear transfer as the trigger to L-H transitions. In the first two panels, the most conventional indicators of the transition, namely, the sudden drop in Balmer-α emission, signifying the decreased plasma-wall interaction, and the increase in electron density at the formation of the pedestal mark the time by which the transition is complete. The sequence of the transition is led by a sharp peak in the term

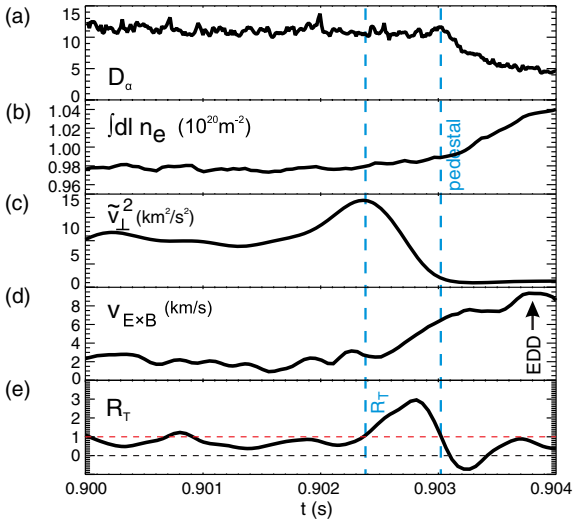

FIG. 2. Key quantities in L-H transitions; (a) $D\alpha$ brightness (A.U.), (b) line-average electron density, (c) turbulent kinetic energy, (d) zonal flow, (e) normalized nonlinear turbulence damping. The first vertical line marks $R_T > 1$, the second one marks the $D\alpha$ drop and the pedestal formation.

$P = \langle \tilde{v}_\theta \tilde{v}_r \rangle \partial_r \langle v_\theta \rangle$, which represents the transfer from turbulence to large-scale flows, gained from the convective derivative in a Reynolds decomposition. In the expression above, v_θ and v_r are the plasma velocities in the poloidal and radial direction, respectively, both perpendicular to the magnetic field $v_\perp^2 = v_r^2 + v_\theta^2$. The critical transfer value at which turbulence is quenched is determined from the balance between P and the effective turbulence drive $\gamma_{\text{eff}} \langle \tilde{v}_\perp^2 \rangle$ as $R_T = P/\gamma_{\text{eff}} \langle \tilde{v}_\perp^2 \rangle = 1$, where estimates of γ_{eff} from the steady L mode using balance to P [23], and from turbulence recovery [24] show a close match. In accordance with that expectation, Fig. 2(c) shows that turbulence drops and the zonal flow accelerates as R_T exceeds unity. Previous experiments [23] further established that this transfer is localized in a narrow radial band inside the last closed flux surface (LCFS). Therefore, all analysis presented here concentrates on the region of transfer, $r_{\text{LCFS}} - r \approx 7$ mm.

Having identified the trigger for the transition as an instance of energy transfer, a predictive model requires understanding of how nonlinearities scale up to where they can overcome flow damping. While P is a reasonable measure for a large and explosive transient, stationary nonlinearities are better studied via bispectra. A Fourier transformation of the convective nonlinearity leads to the following expression of net kinetic energy transfer into "target" frequency f,

$$T_v(f) = \sum_{f_1=-f_N}^{f_N} T_v(f_1, f) = -\sum_{f_1=-f_N}^{f_N} \text{Re}\langle \bar{v}_f^\theta v_{f-f_1}^r \partial_r v_{f_1}^\theta \rangle. \quad (1)$$

In the above, $\langle . \rangle$ is an average over realizations—in this case 2 ms each—which can run over either ensembles or time; error can be reduced by measuring in a long stationary discharge. In addition, the decomposition into "source" frequencies (f_1) in the 2D cross-bispectral form $T_v(f_1, f)$ in Eq. (1) can determine which frequencies participate in driving certain fluctuations. The preference for this (v_θ, v_r) cross bispectrum over bicoherence has been established in earlier works [25] for its sensitivity to the direction of transfer: with the sign convention of Eq. (1), a positive (negative) value means that fluctuations of that target scale are experiencing a net energy gain (loss). While previous studies [26] have validated the approach, they were not able (i) to study plasmas with heating reaching the H mode or any intermediate regimes, (ii) to compare favorable and unfavorable geometries, (iii) to examine a reactor-relevant range of magnetic field and plasma density—which the present work makes its explicit focus.

Experiments were carried out on the Alcator C-Mod tokamak [27] (major radius $R = 0.67$ m, typical minor radius $a = 0.21$ m) with a lower-single-null plasma shape at various currents ($B_\phi = 5.4$ T, $I_p = 0.8$–1.2 MA). The reversal of the grad-B drift was achieved by reversing both the toroidal field and the plasma current between sets of experiments (i.e., not dynamically in the same shot). Auxiliary heating was provided by ion-cyclotron resonance heating (ICRH) with a maximum power of $P_{\rm rf} = 3.75$ MW. Density fluctuations were recorded via GPI viewing the HeI $(3^3D \rightarrow 2^3P)$ $\lambda = 587.6$ nm emission from a local puff. GPI channels image an area of 3.5 (radial) × 3.9 cm (vertical), spanning the LCFS $(0.95 < \psi_n < 1.1)$, with an in-focus spot size of 3.8 mm, located at the most turbulent low-field-side midplane of the tokamak, as shown in Fig. 1. Views are coupled to avalanche photodiodes sampled at 2 MHz.

The time-resolved velocity fields v_r and v_θ required for the calculation of the cross bispectra in Eq. (1) can be obtained from radially and vertically separated views via well-tested velocimetry techniques [23]. Because of the complexity of the spectra in the I mode, fluctuation signals are also filtered to include only $k_\theta < 0$ before performing velocimetry, with a sign convention that puts the frequency–wave-number combination $f > 0$, $k_\theta < 0$ in the electron-diamagnetic flow direction. This is motivated by recent measurements showing the lab frame velocity of the WCM's central frequency to be a fair proxy for the local $\mathbf{E} \times \mathbf{B}$ [19,28]. Details of this correspondence and of directionally filtered velocimetry will be elaborated in a follow-up publication. Here we note that an effective Nyquist frequency of 50 kHz is achieved. Both ZF and GAM are primarily v_θ modes, separated by their frequency ranges: as illustrated in Fig. 3(a), where they are below ~3 (ZF) and at ~20 kHz (GAM). Spectra of poloidal velocity fluctuations are shown here for the I mode as well as the L mode. As has been recorded, GAMs are unique to the I mode in C-Mod; i.e., they do not appear in L-mode

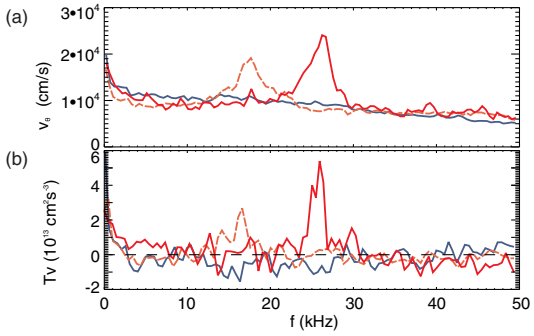

FIG. 3. (a) Poloidal velocity spectra from the favorable L-mode (blue) and two unfavorable I-mode discharges (red). Dashed (solid) lines represent the lower (higher) heating power cases. Note the lack of GAM in the L-mode spectrum.

operation. It is worth noting that the upshift of GAM frequency in the strongly heated discharge is consistent with the mode's frequency dependence $f_{\rm GAM} = c_s/2\pi R = \sqrt{T_e/m_i}/2\pi R$ on temperature.

To investigate the dependences of $T_v(f)$, methodical scans of the heating power were performed. The results of these investigations can be summarized in a single graph shown in Fig. 4. For ease of reference, we first turn our attention to the L mode, i.e., heating below favorable L-H, and the unfavorable L-I transitions, represented in Fig. 4 (left) of the first (red) and second (green) shaded bands, respectively. The L-H threshold is known to depend on plasma density. Measurements of the nonlinear transfer are, therefore, restricted here to a narrow range of $\bar{n}_e = 1.7 \pm 0.15 \times 10^{20}$ m^{-3}. Several models describe ion convected heat flux as dominant in the self-organization of zonal flows. Data are, therefore, organized against the net power flowing across the LCFS, $P_{\rm net} = P_{\rm oh} + P_{\rm rf}^{\rm abs} - dW/dt - P_{\rm rad}$, where $P_{\rm oh}$ is the Ohmic heat generated by the plasma current, $P_{\rm rf}^{\rm abs}$ is the absorbed ICRH, estimated at 80% of coupled power, W is the stored energy, held steady in experiments and $P_{\rm rad}$ is the total radiated

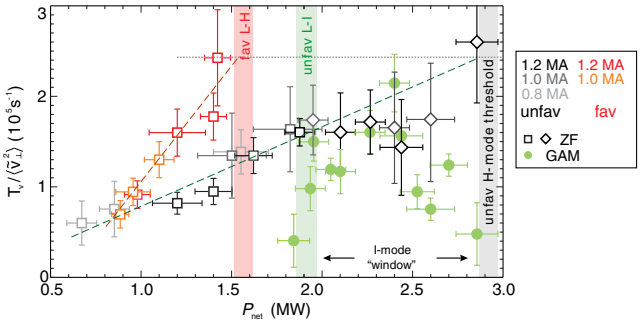

FIG. 4. Nonlinear energy transfer measured from stationary discharges, against net heat flux $P_{\rm net}$. Shades of red represent energy transfer into zonal flows in favorable, gray squares and diamonds represent that in unfavorable L-mode and I-mode plasmas, respectively. Solid (green) circles represent transfer into GAM.

power from the plasma core. The transfer rate is normalized to the velocity fluctuation power to yield an effective nonlinear growth rate $\gamma_{\mathrm{NL}} = T_v/\langle \tilde{v}_\perp^2 \rangle$. The normalization provides for a more direct comparison with R_T quoted in previous work. Results of the power scan confirm that the rates of ZF drive (squares in Fig. 4) show a monotonic, approximately linear increase against P_{net} up to the *L*-*H* transition. Moreover, there is a striking difference between the two geometries, with the "favorable" geometry delivering a larger amount of ZF drive for the same heat flux, as well as a significantly faster increase against P_{net}. The largest spectral transfer, at $\gamma_{\mathrm{NL}} = 2.5 \times 10^5\ \mathrm{s}^{-1}$, measured just below the *L*-*H* threshold, corresponds well to the critical growth rates measured in direct *L*-*H* transitions [23]. Furthermore, since both transfer rate curves can be approximated as linear, γ_{NL} in the unfavorable direction can be extrapolated to stronger heating. It is striking that the extrapolation for the unfavorable geometry reaches the same critical rate at the net power for which the *I*-*H* transition is typically observed. This is consistent with the observation that a reversal in $\mathbf{B} \times \nabla B$ in the *L* mode does not seem significantly to alter the turbulence power or typical scales of turbulence; thus the effective growth time scale γ_{eff} is expected to be the same in both cases, evidence to this is shown in the follow-up to this Letter.

At the studied toroidal field and plasma density, the *L*-*I* transition takes place at a net power slightly above the favorable *L*-*H* transition. A notable difference between the low and high P_{net} regions in Fig. 4 is the presence of GAM above $P_{\mathrm{net}} \approx 1.8$ MW, with measurements of $T_v(f_{\mathrm{GAM}})$ plotted as circles. In a previous study [18], the approximate GAM drive was shown to exceed the neoclassically predicted [29] damping rate, $\gamma_{\mathrm{damp}} = 4\nu_{ii}/(7q)$, at the *L*-*I* transition as the temperature grew and thus the collision frequency ν_{ii} was reduced. Once GAM are present, the GAM drive increases rapidly with P_{net}, with $\gamma_{\mathrm{NL}}(f_{\mathrm{GAM}})$ growing comparable to $\gamma_{\mathrm{NL}}(f_{\mathrm{ZF}})$. Note that the nonlinear transfer into ZF is still measurable in the *I* mode, albeit with increased errors. Measurements are still tracking, within uncertainties, the extrapolation from the *L* mode, and reach the same value of critical transfer rate near the *H*-mode transition. Errors are calculated based on the length of the segment of data used for evaluating T_v, and convergence has been confirmed for all data plotted in Fig. 4 as in Ref. [23]. Since T_v at the GAM frequency converges faster than T_v for the ZF, not all GAM measurement points have a corresponding ZF evaluation. The trend measured in this regime corroborates previous observations [26] of a monotonic, increasing trend of ZF drive with GAM drive shown to peak and decrease against heating. In contrast to Ref. [26], no evidence points to a competition between ZF and GAM en route to direct *L*-*H* transitions, with favorable plasmas not even exciting any measurable GAM in C-Mod. Thus GAMs do not appear to be necessary for producing the *H* mode, which instead relies on the ZF drive.

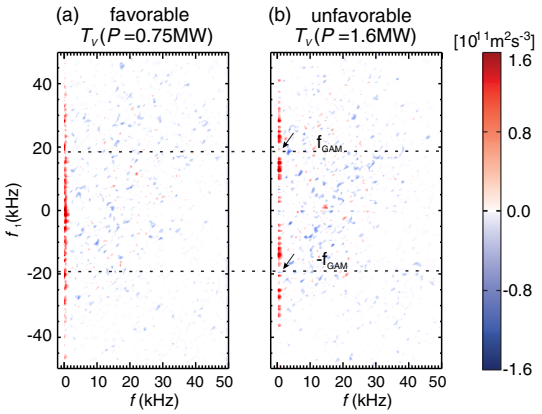

FIG. 5. Frequency-resolved nonlinear energy transfer in favorable (a) and unfavorable (b) geometries at the highest heating power in the *L* mode before a transition. Note gaps in spectrum (b) marked by arrows at $\pm f_{\mathrm{GAM}}$.

However, the competition delineated in Ref. [26] should not be discounted in the *I* mode. While the ZF drive in the *I* mode shows a steady increase, it is impossible to differentiate between a continued linear trend and one which is somewhat dampened by the presence of GAMs. Observations of *I*-*H* transitions triggered by a partial loss of heating, and subsequent cooling in the edge, *are* consistent with the GAM-ZF competition, as GAM damping is more sensitive to this change: in the absence of GAM, zonal flows remain the prime mesoscale feature to be driven by turbulence, and can thus lead to the *H* mode the same way as in an *L*-*H* transition.

One further piece of evidence for this competition is the 2D structure of $T_v(f_1, f)$ in Fig. 5, which highlights the spectral components that contribute to the ZF drive. The clearest contrast can be found between a favorable discharge with heating just below the *L*-*H* threshold and an unfavorable one below the *I* mode. While all resolvable frequencies participate in driving the ZF in the favorable case, shown as the positive (red) band at the target frequency f of ZF, there are two gaps in the equivalent band in the unfavorable case at the frequency where the GAM is about to appear. This indicates that although GAMs are not *yet* driven enough to be observable, the ZF receives no power from the scale dominated by GAMs.

In summary, this Letter reported the first systematic measurement of turbulence nonlinearity on a diverted tokamak with reactor relevant magnetic fields, and the first such scan up to the *H* mode. The nonlinear drive rates of zonal flows are found to be mostly linear as a function of P_{net}. This is the first time that the well-known geometric asymmetry of the *L*-*H* power threshold has been quantitatively assessed in terms of the aforementioned nonlinearity and found to correspond well to the expectations regarding the threshold. The *H*-mode threshold is shown to depend only on the ZF component, with GAM not appearing to be important on the way to the *H*-mode

transition. However, GAM do appear quite important for the *I* mode. The *L*-*I* transition occurs at heating powers below the unfavorable *H*-mode threshold. However, the net heating power needed for appreciable nonlinear GAM drive in the unfavorable geometry is *higher* than the favorable threshold. The *I* mode has always been observed with *both* WCM and GAM activity, with a clear coupling between the two. Thus, it should come as no surprise that the *I* mode is difficult to access in the favorable geometry. All this evidence points to the *I* mode being available in the window which the ZF drive, and the thus *H* mode, leaves for access. The *I* mode exists in the gap where the plasma is hot but cannot yet transition into an *H* mode for lack of ZF support. It still remains to study the fine time scale of the *I*-*H* transition analogously to that of the *L*-*H* transition, as the measurements reported here represent only a clue to the same physics being important in the two situations. Furthermore, it still remains to understand why nonlinear transfer from turbulence to ZF is stronger in the favorable configuration than it is in the unfavorable one. This is perhaps due to neoclassical effects which cause stronger equilibrium shears in one case than the other. The new results are an important step on the road to developing a comprehensive model of phase transitions in plasma turbulence.

The authors thank P. H. Diamond, H. Wilson, and B. Dudson for helpful discussions and suggestions, and the entire Alcator C-Mod team for their help in performing the experiments. This work was performed in partial funding by U.S. Department of Energy, Office of Science, under Awards No. DE-SC-0008689 and No. DE-FC02-99ER54512.

[1] F. Daviaud, J. Hegseth, and P. Bergé, Phys. Rev. Lett. **69**, 2511 (1992).
[2] F. Ravelet, L. Marié, A. Chiffaudel, and F. Daviaud, Phys. Rev. Lett. **93**, 164501 (2004).
[3] F. Wagner, G. Becker, K. Behringer, D. Campbell, A. Eberhagen, W. Engelhardt, G. Fussmann, O. Gehre, J. Gernhardt, G. v. Gierke *et al.*, Phys. Rev. Lett. **49**, 1408 (1982).
[4] J. E. Rice, I. Cziegler, P. H. Diamond, B. P. Duval, Y. A. Podpaly, M. L. Reinke, P. C. Ennever, M. J. Greenwald, J. W. Hughes, Y. Ma, E. S. Marmar, M. Porkolab, N. Tsujii, and S. M. Wolfe, Phys. Rev. Lett. **107**, 265001 (2011).
[5] H. Zohm, Phys. Rev. Lett. **72**, 222 (1994).
[6] L. Schmitz, L. Zeng, T. L. Rhodes, J. C. Hillesheim, E. J. Doyle, R. J. Groebner, W. A. Peebles, K. H. Burrell, and G. Wang, Phys. Rev. Lett. **108**, 155002 (2012).
[7] F. Ryter, W. Suttrop, B. Brsehaber, M. Kaufmann, V. Mertens, H. Murmann, A. G. Peeters, J. Stober, J. Schweinzer, H. Zohm, and A. U. Team, Plasma Phys. Controlled Fusion **40**, 725 (1998).
[8] D. Whyte, A. Hubbard, J. Hughes, B. Lipschultz, J. Rice, E. Marmar, M. Greenwald, I. Cziegler, A. Dominguez, T. Golfinopoulos, N. Howard, L. Lin, R. McDermott, M. Porkolab, M. Reinke, J. Terry, N. Tsujii, S. Wolfe, S. Wukitch, Y. Lin, and the Alcator C-Mod Team Collaboration, Nucl. Fusion **50**, 105005 (2010).
[9] J. A. Snipes and the International H-mode Threshold Database Working Group Collaboration, Plasma Phys. Controlled Fusion **42**, A299 (2000).
[10] P. Gohil, G. R. McKee, D. Schlossberg, L. Schmitz, and G. Wang, J. Phys. Conf. Ser. **123**, 012017 (2008).
[11] G. McKee, P. Gohil, D. Schlossberg, J. Boedo, K. Burrell, J. deGrassie, R. Groebner, R. Moyer, C. Petty, T. Rhodes, L. Schmitz, M. Shafer, W. Solomon, M. Umansky, G. Wang, A. White, and X. Xu, Nucl. Fusion **49**, 115016 (2009).
[12] C. Maggi *et al.*, Nucl. Fusion **54**, 023007 (2014).
[13] E. Righi *et al.*, Nucl. Fusion **39**, 309 (1999).
[14] J. Snipes *et al.*, Nucl. Fusion **36**, 1217 (1996).
[15] S. J. Zweben, D. P. Stotler, J. L. Terry, B. LaBombard, M. Greenwald, M. Muterspaugh, C. S. Pitcher, A. C.-M. Group, K. Hallatschek, R. J. Maqueda, B. Rogers, J. L. Lowrance, V. J. Mastrocola, and G. F. Renda, Phys. Plasmas **9** 1981 (2002).
[16] I. Cziegler, J. L. Terry, J. W. Hughes, and B. LaBombard, Phys. Plasmas **17**, 056120 (2010).
[17] N. Winsor, J. L. Johnson, and J. M. Dawson, Phys. Fluids **11**, 2448 (1968).
[18] I. Cziegler, P. H. Diamond, N. Fedorczak, P. Manz, G. R. Tynan, M. Xu, R. M. Churchill, A. E. Hubbard, B. Lipschultz, J. M. Sierchio *et al.*, Phys. Plasmas **20**, 055904 (2013).
[19] P. Manz, P. Lauber, V. Nikolaeva, T. Happel, F. Ryter, G. Birkenmeier, A. Bogomolov, G. Conway, M. Manso, M. Maraschek, D. Prisiazhniuk, and E. Viezzer, Nucl. Fusion **55**, 083004 (2015).
[20] P. H. Diamond, S. Itoh, K. Itoh, and T. S. Hahm, Plasma Phys. Controlled Fusion **47**, R35 (2005).
[21] Z. Yan, G. R. McKee, R. Fonck, P. Gohil, R. J. Groebner, and T. H. Osborne, Phys. Rev. Lett. **112**, 125002 (2014).
[22] I. Cziegler, G. R. Tynan, P. H. Diamond, A. E. Hubbard, J. W. Hughes, J. H. Irby, and J. L. Terry, Plasma Phys. Controlled Fusion **56**, 075013 (2014).
[23] I. Cziegler, G. Tynan, P. Diamond, A. Hubbard, J. Hughes, J. Irby, and J. Terry, Nucl. Fusion **55**, 083007 (2015).
[24] P. Manz, G. S. Xu, B. N. Wan, H. Q. Wang, H. Y. Guo, I. Cziegler, N. Fedorczak, C. Holland, S. H. Muller, S. C. Thakur, M. Xu, K. Miki, P. H. Diamond, and G. R. Tynan, Phys. Plasmas **19**, 072311 (2012).
[25] M. Xu, G. R. Tynan, C. Holland, Z. Yan, S. H. Muller, and J. H. Yu, Phys. Plasmas **16**, 042312 (2009).
[26] M. Xu, G. R. Tynan, P. H. Diamond, P. Manz, C. Holland, N. Fedorczak, S. C. Thakur, J. H. Yu, K. J. Zhao, J. Q. Dong *et al.*, Phys. Rev. Lett. **108**, 245001 (2012).
[27] I. H. Hutchinson, R. Boivin, F. Bombarda, P. Bonoli, S. Fairfax, C. Fiore, J. Goetz, S. Golovato, R. Granetz, M. Greenwald *et al.*, Phys. Plasmas **1**, 1511 (1994).
[28] C. Theiler, J. L. Terry, E. Edlund, I. Cziegler, R. M. Churchill, J. W. Hughes, B. LaBombard, T. Golfinopoulos, and the Alcator C-Mod Team Collaboration, Plasma Phys. Controlled Fusion **59**, 025016 (2017).
[29] S. V. Novakovskii, C. S. Liu, R. Z. Sagdeev, and M. N. Rosenbluth, Phys. Plasmas **4**, 4272 (1997).